The Influence of Microstructure on Fatigue Crack Propagation Behavior of Stainless Steel Welds

Fatigue tests on controlled samples exhibited a correlation between large grain size and improved crack resistance

BY C. S. KUSKO, J. N. DUPONT, AND A. R. MARDER

ABSTRACT. The influence of microstructure on the fatigue crack propagation behavior of gas metal arc welds in 316L and AL6XN austenitic stainless steels has been investigated. A constant ΔK (stress intensity range) testing procedure with a stress ratio value of 0.6 was first used to deconvolute stress intensity range and residual stress effects from microstructural effects as the fatigue crack propagated from the base metal into the weld metal. The results of this test demonstrated that the large grain size of the weld metal produced a rough fracture surface with improved fatigue resistance relative to the base metal. The influence of grain size on fatigue resistance was then studied in more detail by generating full fatigue curves over a wide range of ΔK on base metal samples that were heat treated to obtain various uniform grain sizes. Results from fatigue tests conducted on the base metal control samples were consistent with the weld metal results and showed that large grain sizes produced relatively rough fracture surfaces with improved fatigue resistance. The improved fatigue resistance occurred predominately at low stress intensity ranges where the plastic zone size is approximately equal to or less than the grain size. The improved fatigue resistance with increasing grain size was attributed to three main factors, including 1) a tortuous crack path that requires formation of a large surface area for a given length of crack propagation, 2) crack growth out of the Mode I plane, which reduces the stress intensity range available for crack growth, and 3) roughness-induced closure that shields the crack from part of the applied load. Direct crack closure measurements were used to identify the range of ΔK levels where the third factor was operable. Quantitative estimates of the ΔK level below which grain size effects are expected to occur are in reasonable agreement with the experimental results.

C. S. KUSKO is Research Assistant; J. N. DUPONT is Associate Professor and Director, Joining and Laser Processing Laboratory; and A. R. MARDER is Professor, Department of Materials Science and Engineering, Lehigh University, Bethlehem, Pa.

Introduction

Stainless steel alloys are used in many applications that are exposed to cyclic loading conditions. In these applications, detailed knowledge of the fatigue crack growth behavior is important for establishing allowable stresses and flaw sizes. In addition, many components are fabricated by welding, so knowledge of the fatigue behavior of the weld is also important.

Although data exist on the fatigue crack growth behavior of stainless steel alloys and their welds (Refs. 1–7), relatively little work has been conducted to determine the influence of weld microstructure on fatigue crack growth in detail. Results obtained to date have shown that the presence of δ-ferrite can influence the nature of the crack propagation path, but this has no significant effect on the actual crack growth rates (Refs. 1–3). It has also been observed that the weld metal often exhibits better fatigue resistance (i.e., lower crack growth rates) compared to the base metal (Ref. 8); however, the reasons for this are not yet clear

Most fatigue testing is conducted using standard ΔK-increasing tests. While such tests are useful for obtaining the direct relation between crack growth rate (da/dN) and stress intensity range (ΔK), it is difficult to understand the role of microstructure on fatigue resistance. For example, in a standard fatigue test conducted on a weld sample, the ΔK level is varied as the crack propagates from the base metal into the weld. In this condition, crack growth rates will change due to varying ΔK, varying residual stress level, and/or changes in microstructure. Thus, with all three factors changing simultaneously, it is difficult to determine the role of weld metal microstructure in detail. An alternative approach to this problem is to use a constant ΔK test (Refs. 9–11). With this approach, a computer-controlled testing algorithm is used that is capable of reducing the applied loads as the crack grows from the base metal into the weld metal so that ΔK remains constant. In addition, a stress ratio, R (R = ratio of minimum-to-maximum stress), is used that is high enough to overcome residual stress effects. At low R values, the crack may enter into a region in which the compressive residual stress is higher than the minimum applied stress. Under this condition, the crack will remain closed during a portion of the stress cycle, which reduces the applied ΔK to some lower, effective ΔK level and causes a reduction in crack growth rate. In order to overcome this effect, higher R values must be used in combination with a method for directly detecting crack closure conditions so that it is ensured the fatigue crack is always open. With this constant ΔK/high R approach, any effects of microstructure on fatigue resistance will readily be signaled by a change in the measured da/dN as the crack propagates across various microstructural zones, thus providing a sensitive method for deconvoluting microstructure effects from residual stress and stress intensity range effects.

In a companion article (Ref. 12), the fatigue crack propagation behavior of stainless steel gas metal arc welds was investigated using a conventional ΔK-increasing testing procedure. A series of stress ratios from 0.10 to 0.80 was investi-

KEY WORDS

Fatigue Crack
GMAW
Austenitic Stainless Steels
Fatigue Resistance
316L Stainless Steel
AL6XN Stainless Steel

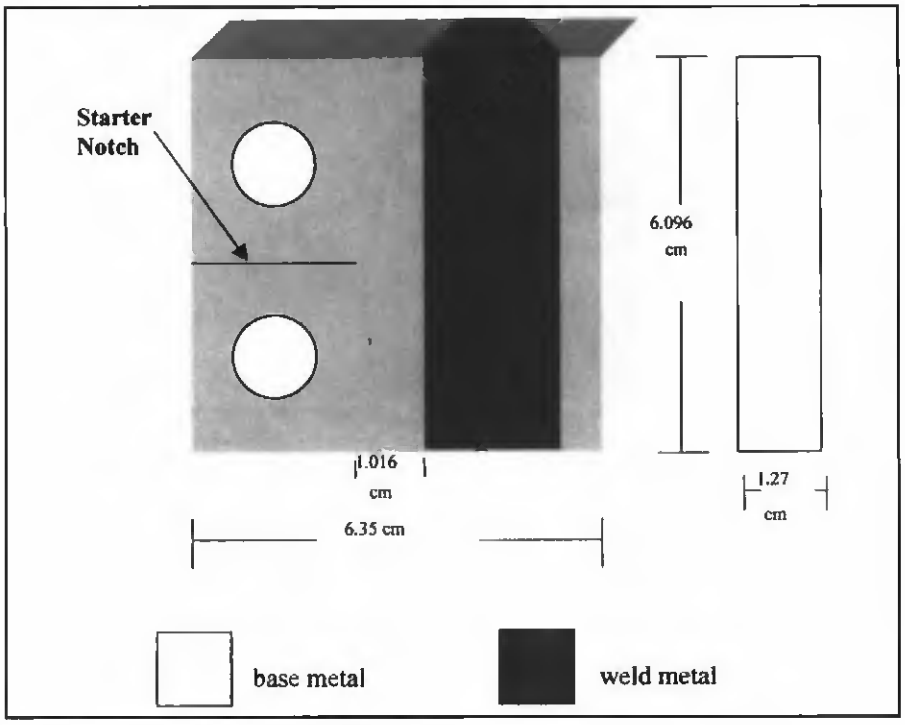

Fig. 1 — Schematic illustration of C(T) specimens.

gated, and crack closure measurements were obtained through a novel compliance offset method. The increase in fatigue crack growth rate that occurred as the stress ratio increased from 0.10 to 0.55 was attributed to an extrinsic crack closure effect in which higher stress ratios promoted a fully open crack and corresponding higher growth rates. Continued increase in the crack growth rate that occurred as the stress ratio increased further from 0.55 to 0.70 was attributed to a true intrinsic material response to increasing stress ratio. These results were useful because they provided a critical stress ratio needed to overcome crack closure effects associated with residual stress.

The purpose of the current research is to use a constant ΔK test procedure in order to determine the influence of microstructure on the fatigue resistance of welds relative to that of the base metal. Once this relative relation was established, full fatigue curves over a larger ΔK range were established for base metals with well-controlled, uniform microstructures in order to investigate the influence of microstructure on fatigue behavior in more detail. The results of this research shed light on the role of weld metal microstructure on fatigue crack growth rate.

Experimental Procedure

Materials and Welding Procedure

The compositions of the base metals and filler metals used in this study are summarized in Table 1. Details of the welding and sample preparation techniques can be found in Ref. 12 and will be briefly described here. Gas metal arc welds (GMAW) were prepared with matching filler metals on each alloy as described in previous work (Ref. 12). It should be noted that matching filler metal for Alloy AL6XN is not typically used in industrial practice. This alloy is typically welded with a nickel-based filler metal enriched in Mo (Ref. 13) to help compensate for Mo microsegregation. However, the objective of this work was to investigate the influence of microstructural variations between the base metal and filler metal at similar compositions. Thus, a special heat of matching AL6XN filler metal was prepared and used for this purpose. Multiple passes were deposited on 19-mm-thick base metals using an automatic welding system with 1.6-mm-diameter filler metal and a wire feed speed of 470 cm/min for the 316L weld and 521 cm/min for the AL6XN weld. The arc current was 280 A, the voltage was approximately 25 V, and the travel speed was 27–33 cm/min for the 316L weld and 41–46 cm/min for the AL6XN weld. All welding was conducted in the flat position using a $98Ar/2O_2$ shielding gas mixture with no preheat and a 150°C interpass temperature. Five layers were used to fill the weld joints with a total of 14 passes.

Both AL6XN and 316L base metal samples were subjected to heat treatments with the intent of increasing the grain size in order to determine the influence of grain size on fatigue crack growth in a controlled manner. Samples were wrapped in stainless steel foil to minimize oxidation during heat treatment and heated at 1250°C for either 45 minutes or 5 hours. The samples were air cooled to room temperature after heat treating. Grain size was measured in accordance with ASTM Standard E112 (Ref. 14). Compact tension (C(T)) specimens were machined from the base metals and welds as shown schematically in Fig. 1. The samples conformed to requirements of ASTM Standard E647 (Ref. 15). A fatigue crack starter notch 2.54 cm in length, with a 0.15 mm diameter, and a 0.077 mm radius of curvature, was inserted into the specimen by wire electrical-discharge machining (EDM). As previously described, the starter fatigue notch in the welds was placed perpendicular to the welding direction.

Table 1 — Chemical Compositions of Base Metals and Filler Metals

	AL6XN Base Metal	316L Base Metal	AL6XN Filler Metal	316L Filler Metal
Ni	24.61	10.16	23.90	12.17
Cr	21.14	16.12	21.30	18.20
Fe	Balance	Balance	Balance	Balance
Mo	6.31	2.05	6.10	2.53
Mn	0.35	1.71	0.20	1.66
Cu	0.26	0.44	—	0.10
Si	0.45	0.41	0.30	0.86
Co	0.18	0.15	—	—
C	0.018	0.017	0.023	0.016
P	0.022	0.027	—	0.017
S	0.0004	0.0011	—	0.014

Note: All values expressed in wt-%.

Fatigue Crack Propagation Testing

Details of the testing procedure can also be found in Ref. 12 and will be briefly reviewed here. All testing was conducted in accordance with ASTM E647 (Ref. 15). An automated, computer-controlled test system was used for testing, acquisition, and reduction of data. Testing was first performed on the welds using a constant ΔK test procedure at a constant R ratio of 0.60. The ΔK level was held constant at 15 $MPa\sqrt{m}$ for the 316L weld and 8 $MPa\sqrt{m}$ for the AL6XN weld. With this method, an algorithm is used to reduce the loads as the crack grows so that the stress intensity range remains constant. This stress ratio of 0.60 was utilized based on earlier work (Ref. 12), which demonstrated that this R value effectively overcomes residual stress effects. Thus, any observed change in fatigue resistance can be attributed to microstructural effects. The fracture surface

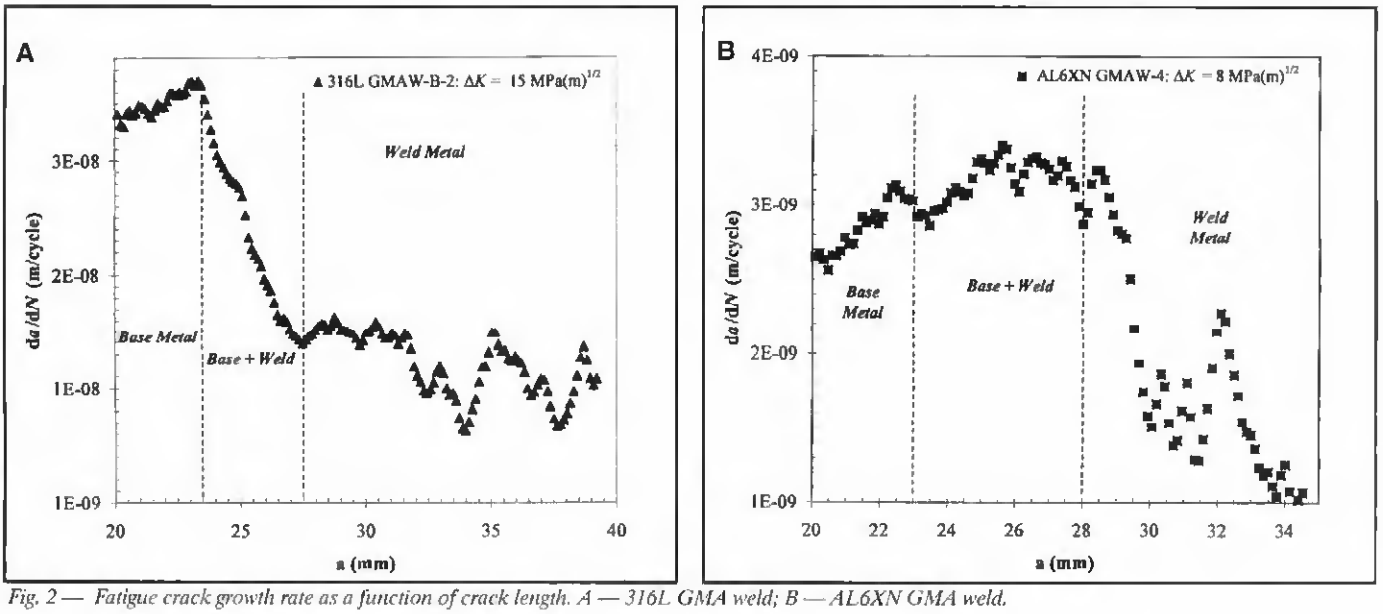

Fig. 2 — Fatigue crack growth rate as a function of crack length. A — 316L GMA weld; B — AL6XN GMA weld.

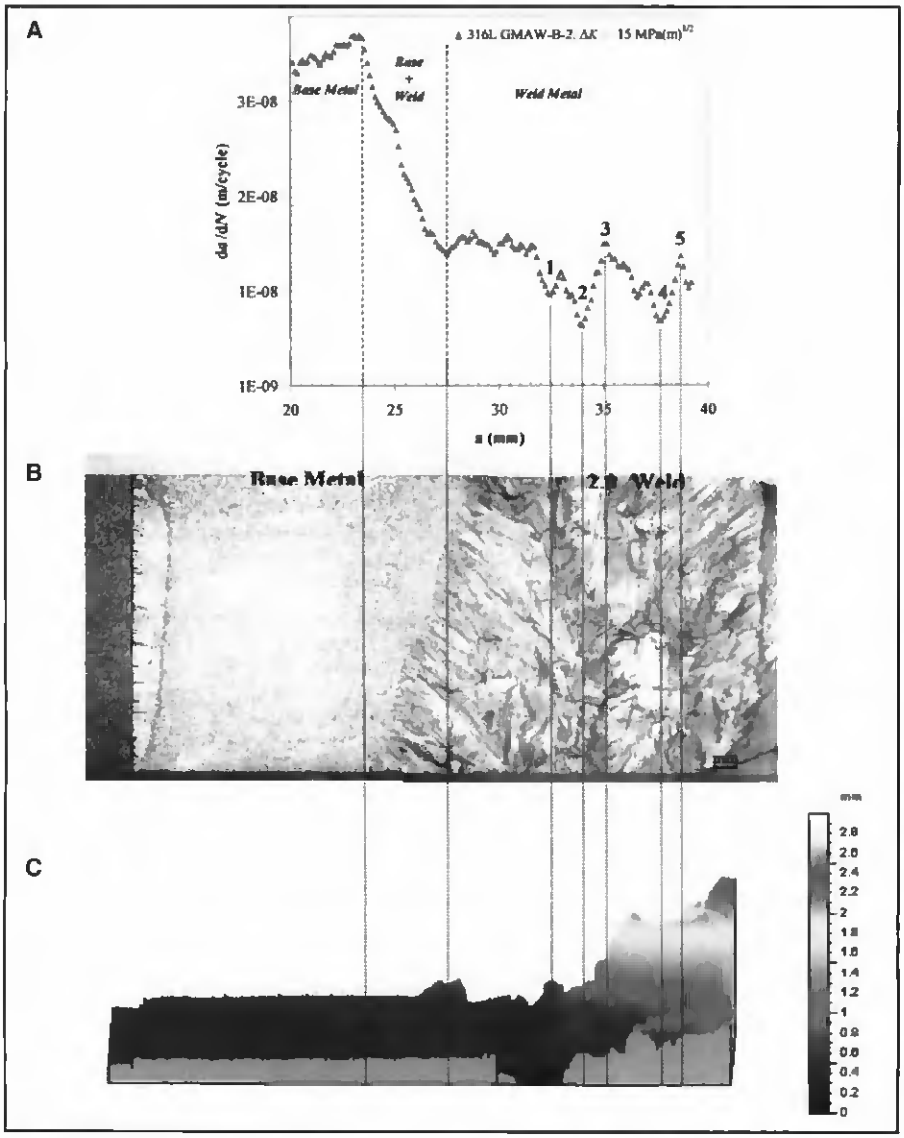

Fig. 3 — Fatigue results from 316L GMA weld constant ΔK test. A — Fatigue results; B — fracture surface; C — surface profile.

roughness of the welds was determined using optical profilometry. Standard fatigue tests with varying ΔK were then conducted on the heat treated base metal samples. Compliance measurements were recorded on both loading and unloading portions of the load-displacement curve. All testing was conducted using constant amplitude loading and a sine waveform at a frequency of 25 Hz at room temperature.

Results

Constant ΔK Test Results

Figure 2 shows the results of constant ΔK results for the weld metals. These results show the variation in fatigue crack growth rate as the weld traverses from the base metal, into the base metal plus weld region, and then into the weld. It is interesting to note that the fatigue resistance of the weld is better than that of the base metal, i.e., the crack growth rate of the weld is lower than that of the base metal. For each weld, it was observed that the weld metal fracture surface was significantly rougher than the base metal. This is shown in more detail in Fig. 3 for the 316L weld.

The fatigue results from Fig. 2A are replotted in Fig. 3A. Figure 3B shows a photograph of the fracture surface, where various locations on the fracture surface are aligned with the corresponding crack growth rates measured in Fig. 3A. The large, columnar grain structure of the weld is readily evident in Fig. 3B. Figure 3C shows results from optical profilometry, which show how the fracture surface roughness changes as the crack propagates from the base metal into the weld metal. As with Fig. 3B, the optical profilometry

results are aligned with the fatigue results so that the variation in surface roughness can be matched with the corresponding crack growth rates. A length scale key is provided on the right of Fig. 3C for reference. These results clearly show that the fatigue resistance of the weld metal is better than that of the base metal and the fracture surface roughness increases significantly as the crack propagates from the base metal into the weld.

The results shown in Figs. 2 and 3 suggest that the large grain size is responsible for the rough fracture surface and concomitant improvement in fatigue resistance. However, the large variation in grain size and columnar grain morphology in the weld make definitive conclusions difficult. Thus, base metal samples with controlled variations in grain sizes were used for fatigue testing to investigate this potential effect in more detail and to determine how grain size influences crack growth rates over a larger applied stress intensity range.

Influence of Grain Size on Fatigue Resistance

Table 2 and Fig. 4 summarize the influence of annealing time on the grain size of 316L and AL6XN stainless steels at 1250°C. Each alloy exhibits similar starting grain sizes. With annealing at 1250°C, the AL6XN grain size is consistently higher at each annealing time. This may be attributed to the small amount of ferrite present in the 316L base metal, which would pin grain boundaries and limit grain growth. The AL6XN alloy, by comparison, is fully austenitic and therefore contains no second phases to restrict grain growth.

Standard fatigue crack growth data, along with ΔK_{eff} data for five slope offset levels, are provided in Figs. 5 and 6 for the base metals of varying grain sizes. The ΔK_{eff} curves are analyzed in the same manner as discussed in previous research in detail (Ref. 12). Briefly, the presence of unique curves for each slope offset level indicates that crack closure is occurring while a single, coincident curve represents a fatigue crack that is fully open. For example, the fatigue results for 316L tested in the as-received condition with a grain size of 24 μm (Fig. 5A) show all offset curves are coincident for all the offset slope levels (which gives the appearance of a single curve) over the entire range of da/dN, indicating that crack propagation has occurred free of closure for all ΔK levels. In this case, the applied ΔK and effective ΔK are equivalent since the crack is always fully open. By comparison, the results generated on 316L base metal with grain sizes of 103 μm and 147 μm (Fig. 5B and C) exhibit crack closure up to approximately 7×10^{-10} m/cycle (Fig. 5B) and 2×10^{-9} m/cycle (Fig. 5C), respectively. (The range of da/dN where closure occurs is indicated in each figure.) Thus, as grain size increases, crack closure effects become evident at higher crack growth rates and corresponding ΔK values. Similar effects are observed for the AL6XN alloy in Fig. 6, although the influence of grain size on crack closure is not as large as that observed in 316L stainless steel. In this case, crack closure is observed below approximately 3×10^{-10} m/cycle for the AL6XN sample with a 210-μm grain size (Fig. 6B) and 6×10^{-10} m/cycle for the sample with a 280-μm grain size — Fig. 6C. The unique offset curves in Fig. 6B are difficult to identify from the figure, but direct inspection of the corresponding numerical data indicates an appreciable level of crack closure in this growth rate range.

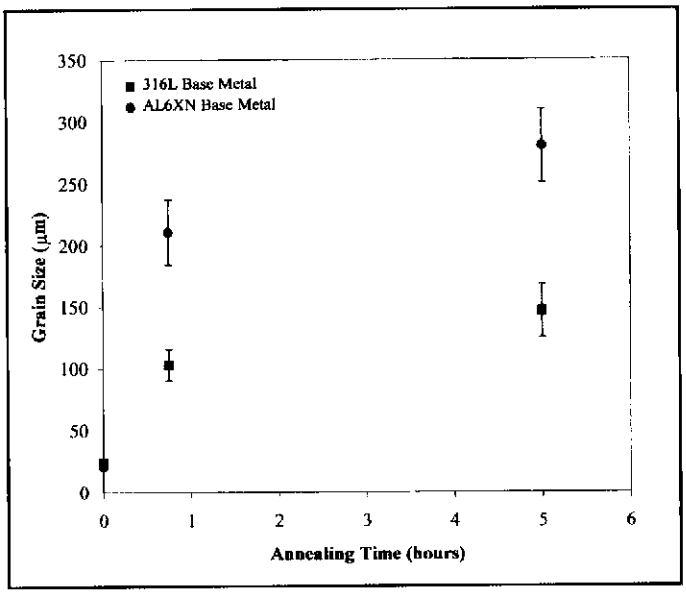

Fig. 4 — Grain size as a function of annealing time at 1250°C for 316L and AL6XN stainless steel base metals.

Figure 7 summarizes the applied da/dN-ΔK curves for the various grain sizes of each alloy. Two fatigue curves were produced for each base metal in the starting condition (smallest grain size) in order to demonstrate reproducibility of the test results. The data in this figure demonstrate the significant influence of grain size on fatigue resistance. Specifically, as the grain size increases, the crack growth rate decreases for a given applied stress intensity range. The reduction in crack growth rate with increasing grain size is particularly evident at low levels of applied stress intensity range near the threshold regime. The crack growth rates then become similar as the applied stress intensity range and concomitant crack growth rates increase to high values. The ΔK_{GS} values noted in Fig. 7 will be discussed in the next section.

Table 2 — Summary of Grain Size Measurements for 316L and AL6XN Stainless Steels after Heat Treating at 1250°C

Condition	Average Grain Size (μm) 316L	AL6XN
As-received	24 ± 3.3	21 ± 2.4
Annealed: 1250°C – 45 minutes	103 ± 12.8	211 ± 26.3
Annealed: 1250°C – 5 hours	147 ± 21.6	280 ± 29.7

Table 3 — Summary of ΔK_{th} Values and Number of Data Points Utilized for ΔK_{th} Calculations

Test Identification	Grain Size (μm)	ΔK_{th} (MPa$\sqrt{m}$)	Number of Data Points between 10^{-10} and 10^{-9} m/cycle
AL6XN–As Received-1	21 ± 2.4	4.2	22
AL6XN–As Received-2	21 ± 2.4	4.4	19
AL6XN–Annealed 45 min.	211 ± 26.3	6.5	24
AL6XN–Annealed 5 h	281 ± 29.7	8.5	12
316L–As Received-1	24 ± 3.3	3.2	28
316L–As Received-2	24 ± 3.3	2.9	26
316L–Annealed 45 min.	103 ± 12.8	4.3	24
316L–Annealed 5 h	147 ± 21.6	5.6	19

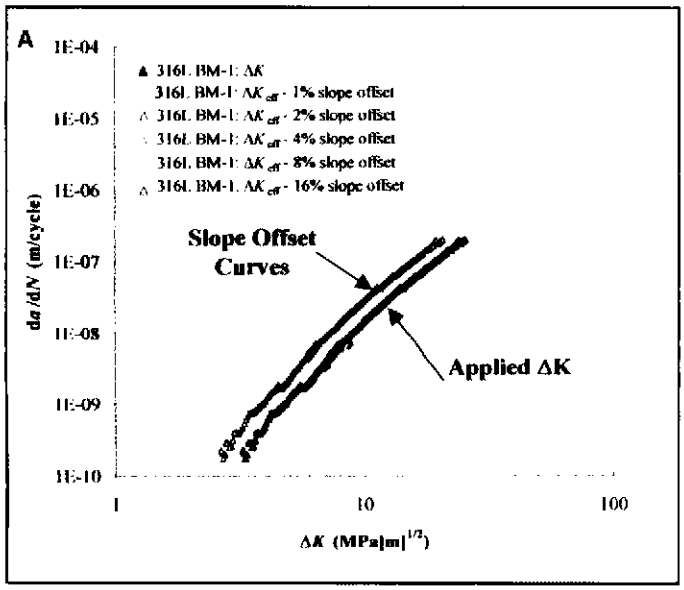

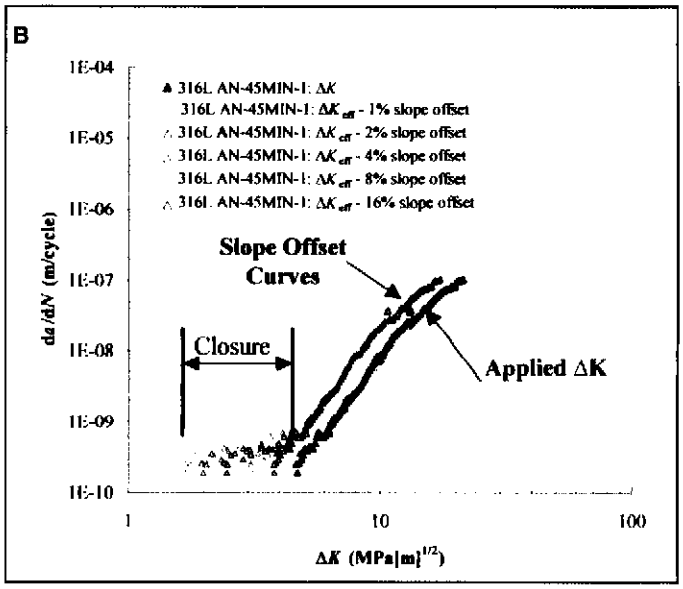

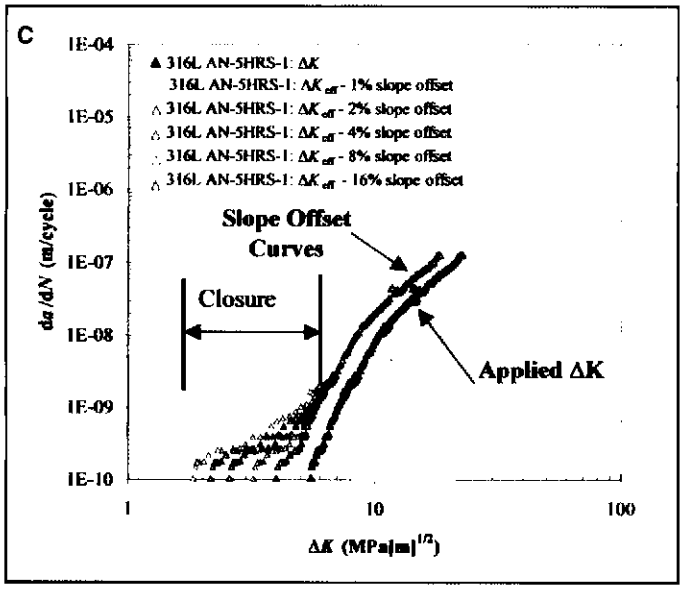

Fig. 5 — Fatigue results and slope offset data. A — 316L base metal with a 24-μm grain size tested at an R ratio of R = 0.60; B — 316L base metal with a 103-μm grain size tested at an R ratio of R = 0.60; C — 316L base metal with a 147-μm grain size tested at an R ratio of R = 0.60.

The threshold stress intensity factor range, ΔK_{th}, can be determined from the fatigue data presented in Fig. 7. The value of ΔK_{th} is defined by ASTM as the ΔK value corresponding to a crack growth rate of 1.00×10^{-10} m/cycle (Ref. 15). ΔK_{th} values for the 316L and AL6XN base metals of varying grain sizes are presented in Table 3. The ASTM Standard E647 requires that determination of ΔK_{th} be completed by conducting a linear regression analysis of the da/dN-ΔK plot with a minimum of five data points between 1.00×10^{-10} m/cycle and 1.00×10^{-9} m/cycle. Therefore, Table 3 also lists the total number of data points between 1.00×10^{-10} m/cycle and 1.00×10^{-9} m/cycle that were used in the analysis. Figure 8 shows the relation between ΔK_{th} and grain size, where it is evident that large grain size favorably increases the threshold stress intensity range.

As with the weld metal, the fracture surface roughness of the base metals increased with increasing grain size. Figure 9 shows an example of this for the AL6XN base metal. These photomicrographs were each acquired from the sample at points where the crack growth rates were similar at ~ 1.5×10^{-10} m/cycle, and crack growth occurred from left to right in the figures. The base metal tested at a grain size of 21 μm (Fig. 9A) exhibits a fracture surface that is relatively flat compared to the sample with a grain size of 210 μm (Fig. 9B), which exhibits a rougher fracture surface.

Discussion

The results presented above demonstrate that the large grain size present in the weld metal provides an increase in the fatigue resistance relative to the base metal, and the improved fatigue resistance is associated with a rough fracture surface. The control tests conducted on the base metals of varying grain size confirm that large grain sizes are beneficial for fatigue resistance, particularly at low crack growth rate regimes.

Fracture surfaces that form with significant surface roughness can improve fatigue resistance in three ways. First, the high surface roughness presents a tortuous crack path that effectively requires formation of a larger fracture surface area for a given length of crack propagation that is orientated perpendicular to the loading direction (compared to relatively flat cracks). In other words, more surface area must be created for a given effective crack length. Second, the crack growth plane can deviate out of the plane that is normal to the applied stress (i.e., out of the Mode I plane). This effectively reduces the stress intensity range that is available to drive the crack and, thus, reduces the crack propagation rate. For example, if Θ is designated as the angle between the crack plane and the Mode I plane, then the stress intensity range that drives crack growth is reduced from ΔK to $\Delta K\cos(\Theta)$ when the crack deviates out of the Mode I plane by an angle of Θ. Lastly, rough fracture surfaces can induce crack closure. In this case, large asperities on the mating halves of the fracture surface come into contact with one another during the unloading portion of the curve. This causes the crack to partially close, which shields the crack from part of the applied load and reduces the stress intensity range available for crack growth.

It is evident from Fig. 7 that the beneficial effect of large grain size is most operable at low levels of applied stress intensity range. This is consistent with the three mechanisms described above, since all of these mechanisms occur predominately at low ΔK levels. First consider the

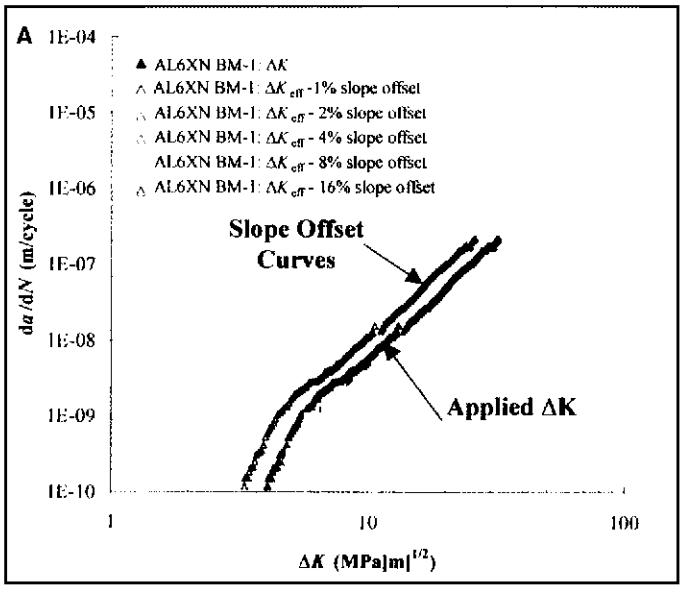

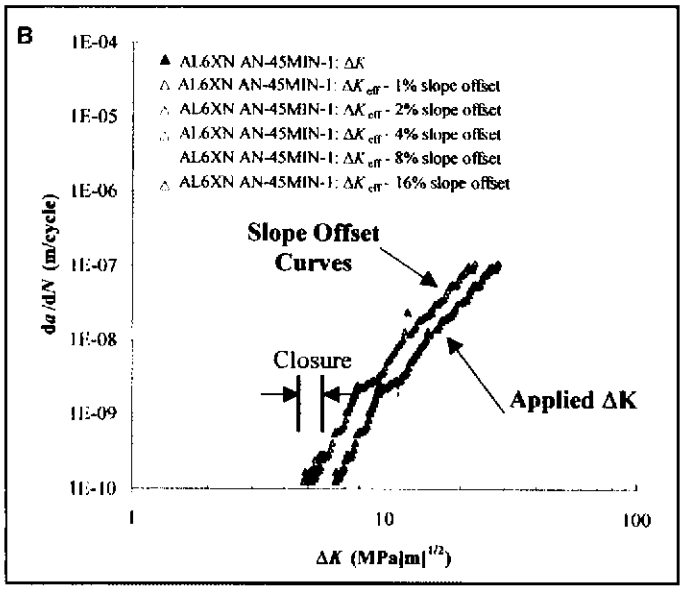

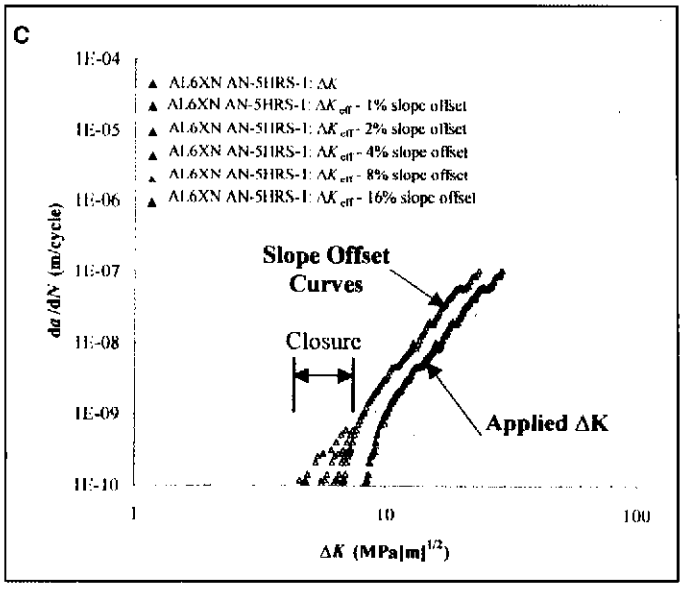

Fig. 6 — Fatigue results and slope offset data. A — AL6XN base metal with a 21-μm grain size tested at an R ratio of R = 0.60; B — AL6XN base metal with a 211-μm grain size tested at an R ratio of R = 0.60; C — AL6XN base metal with a 280-μm grain size tested at an R ratio of R = 0.60.

influence of crack closure. As the loads are reduced in order to reduce ΔK during development of a full fatigue curve, the crack opens a proportionally lesser amount and the mating surfaces come closer to each other during the unloading portion of the fatigue cycle. Eventually, the loads can be reduced to the point where the asperities of mating fracture surfaces can come into contact if the fracture surface exhibits enough roughness. This shields the crack from a portion of the applied load and effectively reduces the stress intensity range available to drive crack growth. In fact, the closure measurements made during fatigue testing of the base metals (Figs. 5 and 6) provide an indication of the ΔK level at which crack closure contributes to the improved fatigue resistance. These conditions were described in the Results section and are summarized in Table 4. The ΔK values in Table 4 indicate the stress intensity range at which crack closure occurs as ΔK is reduced. Note that the values shown in Table 4 increase as the grain size increases, which indicates that closure effects occur at higher ΔK levels as the grain size increases. This is in direct response to the rougher fracture surface that forms with increasing grain size. Thus, crack closure is at least one cause of the improved fatigue resistance for crack growth rates below the ΔK values summarized in Table 4. It should be noted that crack closure can also occur due to residual stress effects as discussed in previous work (Ref. 12). However, these tests were conducted on samples that were slowly heated and cooled during the grain growth treatments, so significant residual stress is not expected in these samples. In addition, previous work (Ref. 12) has demonstrated that residual effects in these alloys are overcome with the R value of 0.6 that is used here.

The remaining two mechanisms that account for improved fatigue resistance (deviation of the crack plane out of the Mode I plane and creation of more surface area for a given crack length) can be attributed to crystallographic effects on the fatigue crack growth. It has been established (Ref. 16) that fatigue crack growth occurs on preferred crystallographic planes when the plastic zone size that develops during growth is approximately equal to or less than the grain size. The plastic zone size (r_{cyc}), in turn, is controlled by the yield strength (σ_{ys}) and applied ΔK and can be estimated by (Refs. 16–18)

$$r_{cyc} = 0.033\left(\frac{\Delta K}{\sigma_{ys}}\right)^2 \qquad (1)$$

For a given material, the plastic zone size decreases with decreasing ΔK. Thus, as ΔK is reduced during the fatigue test, a point is eventually reached when the plastic zone size approaches (and eventually becomes smaller then) the grain size. Under this condition, crack growth occurs along preferred crystallographic planes, even though that direction may not be oriented within the Mode I plane. In austenitic stainless steels, growth is favored predominantly on {111} planes (Refs. 19, 20). Crack growth occurs along such favorable planes until reaching a neighboring grain of different crystallographic orientation. The crack is then forced to find the favorably oriented plane for continued propagation into the neighboring grain. When this process occurs in large grained materials, the cracks may extend farther distances along the favorable planes and out of the Mode I plane prior

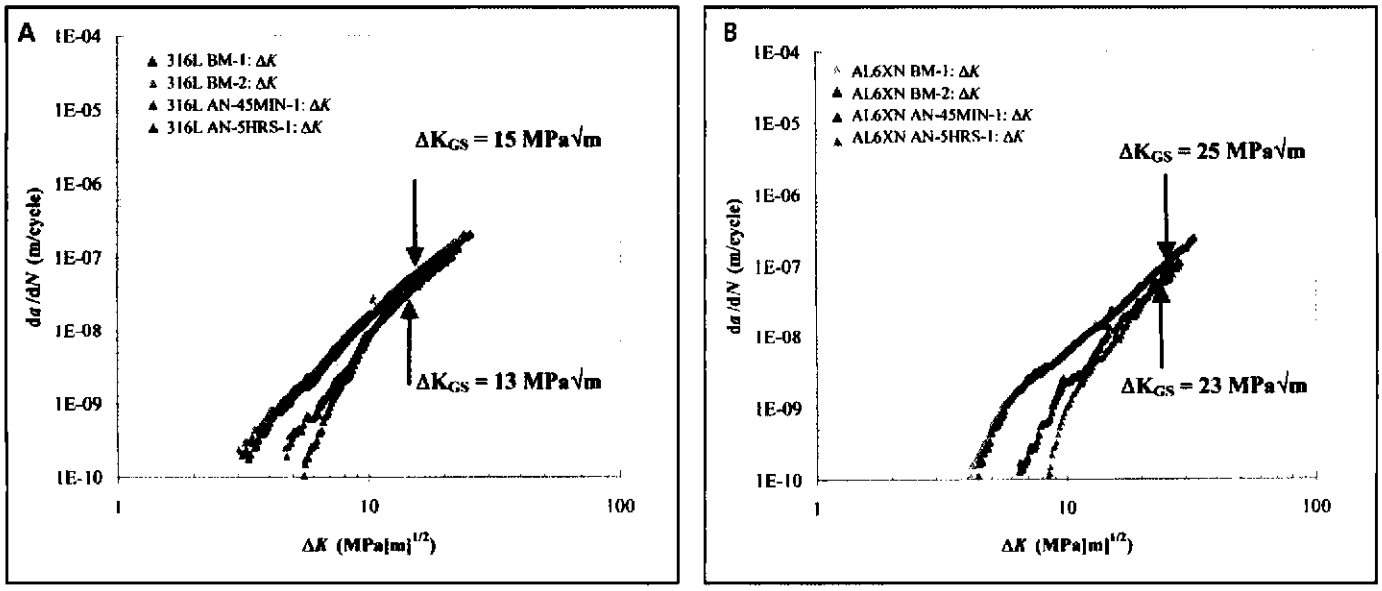

Fig. 7 — Applied da/dN-ΔK curves for various grain sizes. A — 316L; B — AL6XN.

Table 4 — Summary of ΔK Levels below Which Crack Closure Was Observed

Grain Size (μm)	ΔK below which closure was observed, (MPa√m)
316L Stainless Steel	
24 ± 3.3	No closure observed
103 ± 12.8	7×10^{-10}
147 ± 21.6	2×10^{-9}
AL6XN Stainless Steel	
21 ± 2.4	No closure observed
211 ± 26.3	3×10^{-10}
281 ± 29.7	6×10^{-10}

Table 5 — Summary of Grain Sizes and Calculated Yield Strengths for 316L Stainless Steel

Sample	d (μm)	σ_{ys} (MPa) M-Measured C-Calculated	ΔK below Which Grain Size Effects Are Expected, MPa√m
316L–As received	24 ± 3.3	320-C 306-M	8
316L–Annealed 45 min.	103 ± 12.8	239-C	13
316L–Annealed 5 h	147 ± 21.6	227-C	15
AL6XN–As received	21 ± 2.4	397-M	10
AL6XN–Annealed 45 min	211 ± 26.3	282-C	23
AL6XN–Annealed 5 h	281 ± 29.7	275-C	25

to changing their path. The expected result would be a tortuous crack path, as observed experimentally in this study.

Equation 1 can be used with known σ_{ys} values to estimate the ΔK value below which these grain size effects are expected to occur. This value of ΔK is denoted at ΔK_{GS} for reference. By setting the plastic zone size (given by Equation 1) equal to the grain size, the ΔK value below which grain size effects are expected to occur is given as

$$\Delta K_{GS} = \sigma_{ys}\left[\frac{d}{0.033}\right]^{\frac{1}{2}} \qquad (2)$$

Where d is the grain size. There was insufficient material available to directly determine the yield strength of all the samples as a function of grain size. However, knowledge of the yield strength of the as-received 316L and AL6XN provide two useful data points. In addition, Hall-Petch parameters established for the 316L alloy permit a good estimate of the yield strength as a function of grain size for this alloy. Priddle (Ref. 21) previously established the influence of grain size on yield strength with the following Hall-Petch equation for 316L stainless steel:

$$\sigma_{ys} = \sigma_o + \frac{k_d}{\sqrt{d}} \qquad (3)$$

in which σ_o = 163 MPa and k_d = 0.77 MPa√μm. Equation 3 produces very good agreement between calculated (320 MPa) and measured (306 MPa) σ_{ys} values for 316L in the as-received condition (5% error). Although no Hall-Petch relation was available in the literature for AL6XN, Equation 3 can be used to at least estimate the expected change in yield strength with grain size for AL6XN. Here, it is assumed that the incremental change in σ_{ys} with d is similar to 316L (i.e., the k_d constant in Equation 3 is identical), and that the net variation in σ_{ys} can be accounted for by the σ_o term in Equation 3. With this assumption, the σ_o term in Equation 3 can be determined so that agreement is found between the starting grain size (d = 21 μm) and yield strength (σ_{ys} = 397 MPa) of AL6XN. A σ_o value of 229 MPa provides this agreement. Thus, the following two Hall-Petch equations were used to determine yield strength as a function grain size

$$\sigma_{ys} = 163 + \frac{0.77}{\sqrt{d}} \qquad (4)$$

for 316L stainless steel

$$\sigma_{ys} = 229 + \frac{0.77}{\sqrt{d}} \qquad (5)$$

for AL6XN stainless steel

where d is in μm. Table 5 summarizes σ_{ys} values calculated for each grain size for each alloy. Also shown in the table are the ΔK_{GS} values below which grain size effects

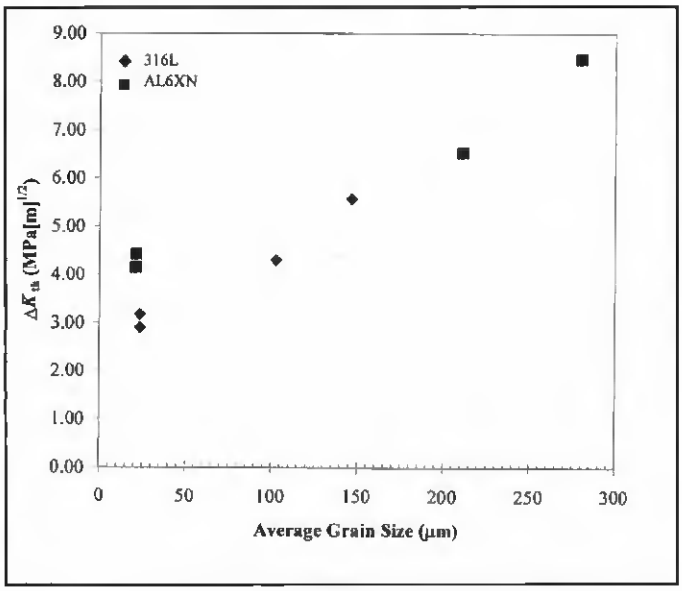

Fig. 8 — Variation in threshold stress intensity range, ΔK_{th}, as a function of grain size.

Fig. 9 — Comparison of fracture surface roughness in AL6XN base metal samples with various grain sizes. A — Grain size is 21 μm and crack growth rate is 1.5×10^{-10} m/cycle at arrow; B — grain size is 211 μm and crack growth rate is 1.7×10^{-10} m/cycle at arrow location.

are expected to occur as ΔK is reduced. This ΔK_{GS} value becomes larger with increasing grain size. In other words, grain size will improve fatigue resistance over a larger range of ΔK as the grain size increases. The interpretation of these values is shown schematically in Fig. 10 for three materials with three different grain sizes (where $d^3 > d^2 > d^1$). The corresponding ΔK values at which grain size effects begin to occur with decreasing ΔK are denoted as ΔK^3_{GS}, ΔK^2_{GS}, and ΔK^1_{GS} (where $\Delta K^3_{GS} > \Delta K^2_{GS} > \Delta K^1_{GS}$).

As previously explained, the plastic zone size will increase with increasing ΔK. As this occurs, a point will eventually be reached where the plastic zone size becomes appreciably larger than the grain size and any improvement in fatigue resistance due to grain size diminishes. Thus, the fatigue curves of materials with various grain sizes will eventually coincide as ΔK is increased. This type of behavior is shown schematically in Fig. 10 and, more importantly, is also observed in the experimental data of Fig. 7. In addition, material with the largest grain size will provide improved fatigue resistance over a large range of ΔK. Again, this general trend is also observed in the experimental data of Fig. 7. With this background, it also becomes clear that the various ΔK_{GS} values can be positioned as shown on the schematic fatigue curve provided in Fig. 10. For example, ΔK^3_{GS} represents the ΔK value at which the fatigue curves for alloys with grain sizes of d^3 and d^2 will begin to deviate as ΔK is reduced, and ΔK^2_{GS} represents the ΔK value at which the fatigue curves for alloys with grain sizes of d^2, and d^1 will begin to deviate as ΔK is reduced. A fourth alloy with the finest grain size d^4 would be needed to plot ΔK^1_{GS} in Fig. 10.

The calculated values of ΔK_{GS} from Table 5 are plotted in Fig. 7. The separation of experimental fatigue curves with decreasing ΔK is not nearly as sharp as the schematic curves shown in Fig. 10, which makes exact determination of an experimental ΔK_{GS} value difficult. However, there is generally good agreement between the ΔK_{GS} values that are calculated with Equation 3 and those observed experimentally in Fig. 7. For example, the AL6XN samples that were heat treated to produce the two largest grain sizes (211 and 281 μm) separate from the as-received sample with a 21-μm grain size near the calculated value of ΔK_{GS} = 25 MPa√m. Similarly, the sample with the 281-μm grain size begins to deviate from the 211 grain size sample near the calculated value of ΔK_{GS} = 23 MPa√m. These general trends between measured and calculated ΔK_{GS} values are also evident for the 316L alloy. Again, the deviations in the experimental curves are very gradual, but the reasonable agreement between measured and calculated ΔK_{GS} values provides support for the grain size mecha-

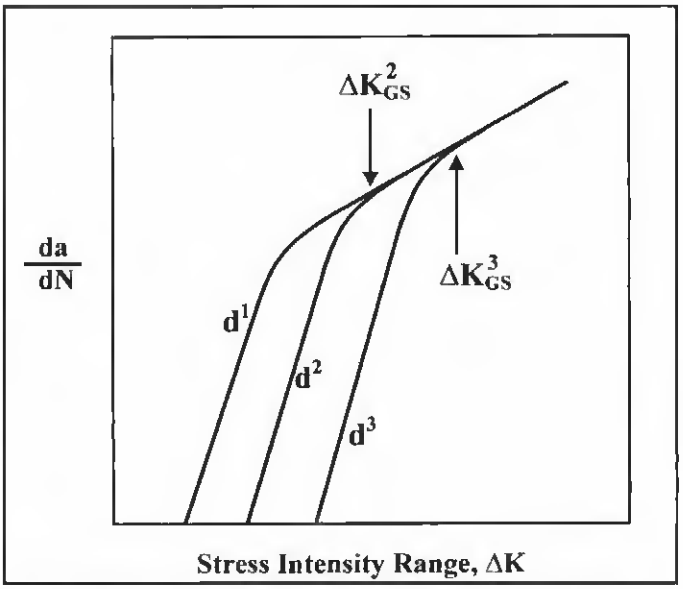

Fig. 10 — Schematic illustration showing the influence of grain size on fatigue crack growth rate. The curves labeled d^3, d^2, and d^1 are for three alloys with grain sizes (d) in which $d^3 > d^2 > d^1$.

nisms to fatigue improvement described above.

Conclusions

The influence of microstructure on the fatigue crack propagation behavior of gas metal arc welds and base metals of 316L and AL6XN austenitic stainless steel has been investigated using conventional fatigue testing and constant ΔK testing procedures. The following conclusions can be drawn from this research:

1) Large grain sizes in both the weld metal and base metal produce a rough fracture surface that leads to improved fatigue resistance.

2) The observed improvement in fatigue resistance occurs at low stress intensity ranges when the plastic zone size is approximately equal to or less than the grain size.

3) The improved fatigue resistance with increasing grain size can be attributed to three main factors: 1) a tortuous crack path that requires formation of a larger surface area for a given length of crack propagation, 2) crack growth out of the Mode I plane, which reduces the stress intensity range available for crack growth, and 3) roughness induced closure that shields the crack from part of the applied load.

4) Quantitative estimates of the ΔK level below which grain size effects are expected to occur are in reasonable agreement with the observed experimental results.

Acknowledgments

The authors thank the United States Office of Naval Research for providing funding for this research. The authors would also like to acknowledge Mike Rex, John Gregoris, and Gene Kozma at Lehigh University for assistance with fatigue crack propagation sample preparation and testing and Arlan Benscoter for assistance with metallography. The authors also gratefully acknowledge Ravi Menon of Stoody Company for preparation of the welds.

References

1. James, L. A. (A) 1973. Crack propagation behavior in Type 304 stainless steel weldments at elevated temperature. *Welding Journal* 52: 173-s to 179-s.

2. James, L. A., and Mills, W. J. 1987. Fatigue crack propagation behavior of Type 316 (16-8-2) weldments at elevated temperature. *Welding Journal* 66: 229-s to 234-s.

3. Provenzano, V., Hawthorne, J. R., and Sprague, J. A. 1978. Properties of steel weldments for elevated temperature pressure containment applications. Ed. G. V Smith, The American Society of Mechanical Engineers: New York, pp. 63–75.

4. Shahinian, P., Smith, H. H., and Hawthorne, J. R. 1972. Fatigue crack propagation in stainless steel weldments at high temperature *Welding Journal* 51: 527-s to 532-s.

5. Raske, D. T., and Cheng, C. F. 1977. *Nuclear Technology* 34: 101–110.

6. Hawthorne, J. R. 1978. Naval Research Laboratory Report 8201.

7. Lloyd, G. J., and Walls, J. D. 1980. *Engineering Fracture Mechanics* 13: 897–911.

8. Pickard, A. C., Ritchie, R. O., and Knott, J. F. 1975. *Metals Technology* 2: 253–263.

9. Dowse, K. R., and Richards, C. E. 1971. *Metallurgical Transactions* 2: 599–603.

10. Griffiths, J. R., Mogford, I. L., and Richards, C. E. 1971. *Metal Science Journal* 5: 150–154.

11. Shih, Y. W., Chen, B. Y., and Zhang, J. X. 1990. *Engineering Fracture Mechanics* 36: 893–902.

12. Kusko, C. S., DuPont, J. N., and Marder, A. R. 2003. To be published in the February 2004 *Welding Journal*.

13. Banovic, S. W., DuPont, J. N., and Marder, A. R. 2003. Dilution and microsegregation in dissimilar metal welds between super austenitic stainless steels and Ni base alloys. *Science & Technology of Welding and Joining* 6(6): 374–383.

14. American Society for Testing and Materials. 1996. ASTM E112. *Annual Book of ASTM Standards*. Section 3: Metals test methods and analytical procedures. 03.01: 226–248.

15. American Society for Testing and Materials. 1998. ASTM E647. *Annual Book of ASTM Standards*. Section 3. Metals test and analytical procedures. 3.01: 565–601.

16. Yoder, G. R., Cooley, L. A., and Crooker, T. W. (B) 1977. *Metallurgical Transactions A* 8A: 1737–1743.

17. Yoder, G. R., Cooley, L. A., and Crooker, T. W. 1978. *Metallurgical Transactions A* 9A: 1413–1420.

18. Yoder, G. R., Cooley, L. A., and Crooker, T. W. (A) 1977. *Journal of Engineering Materials and Technology* 99: 313–318.

19. Priddle, E. K., and Walker, F. E. 1976. *Journal of Materials Science* 11: 386–388.

20. Pedron, J. P., Diboine, A., and Pineau, A. 1984. *Fatigue and Fracture of Engineering Materials and Structures* 7: 137–143.

21. Priddle, E. K. 1978. *Scripta Metallurgica* 12: 49–56.